

## Internal instability of thin liquid sheets

V. Nagabhushana Rao and K. Ramamurthi

Citation: *Physics of Fluids* (1994-present) **21**, 092106 (2009); doi: 10.1063/1.3234190

View online: <http://dx.doi.org/10.1063/1.3234190>

View Table of Contents: <http://scitation.aip.org/content/aip/journal/pof2/21/9?ver=pdfcov>

Published by the [AIP Publishing](#)

---

### Articles you may be interested in

[Thin film lubrication dynamics of a binary mixture: Example of an oscillatory instability](#)

*Phys. Fluids* **22**, 104102 (2010); 10.1063/1.3489434

[A mechanism of Marangoni instability in evaporating thin liquid films due to soluble surfactant](#)

*Phys. Fluids* **22**, 022102 (2010); 10.1063/1.3316785

[Absolute and convective instability of a radially expanding liquid sheet](#)

*Phys. Fluids* **15**, 1745 (2003); 10.1063/1.1570422

[Marangoni instability at a contaminated liquid–vapor interface of a burning thin film](#)

*Phys. Fluids* **15**, 1122 (2003); 10.1063/1.1562939

[Nonlinear dynamics of three-dimensional long-wave Marangoni instability in thin liquid films](#)

*Phys. Fluids* **12**, 1633 (2000); 10.1063/1.870415

---



Zaber's wide range of precision positioning devices are:

**ZABER**

- ❖ Low-cost
- ❖ Easy to set up
- ❖ Simple to use
- ❖ Integrated, with built-in controllers

Learn more at [www.zaber.com](http://www.zaber.com) →

## Internal instability of thin liquid sheets

V. Nagabhushana Rao and K. Ramamurthi<sup>a)</sup>

*Department of Mechanical Engineering, IIT Madras, Chennai 600036, India*

(Received 1 February 2009; accepted 29 August 2009; published online 21 September 2009)

Linear stability analysis of an inviscid liquid sheet with different velocity profiles across its thickness is reported. The velocity profiles for which there is a progressive increase or decrease in velocities between the two interfaces are demonstrated to be inherently unstable even in the absence of the destabilizing aerodynamic shear at the liquid-gas interfaces. Compared to a flat velocity profile, a linear or a parabolic profile, symmetric at the center line of the sheet reduced both the maximum growth rate and the wavelength range over which the waves grow. The convective acceleration from the velocity gradient is found to stabilize longer waves while the growth of shorter waves is hampered by the combined effect of the surface tension and a decrease in the interface velocity between gas and liquid media. The wave forms are dominantly sinuous for symmetric velocity profiles; however, with larger velocity gradients the dilatational modes are observed. The inherent instability of liquid sheets with a progressive change in velocities between the interfaces is seen to arise from the differential convective acceleration at the two interfaces in the plane of reference of the liquid sheets. © 2009 American Institute of Physics. [doi:10.1063/1.3234190]

### I. INTRODUCTION

Several investigations starting with the classic work of Squire<sup>1</sup> have addressed the conditions for the growth of small amplitude disturbances on the surface of liquid sheets. Aerodynamic forces arising from the interaction of the sheet with the surrounding gas medium were found to be the principal sources of instability, while the surface tension effects always tend to smooth out any protuberances.

Hagerty and Shea<sup>2</sup> showed the possibility of sinuous (antisymmetric) and dilatational (symmetric) modes of wave growth at a given frequency. The sinuous and dilatational modes are sketched in Fig. 1. The growth rate of sinuous mode is generally greater than the dilatational mode. Rangel and Sirignano<sup>3</sup> showed the growth rate of dilatational mode to dominate over sinuous mode at higher values of gas to liquid density ratios.

Although the sinuous mode was found to generally dominate, the importance of dilatational mode was brought out in the nonlinear stability analysis carried out by Jazayeri and Li.<sup>4</sup> The effect of higher harmonics on the fundamental sinuous mode was studied by a perturbation expansion technique, choosing the initial disturbance amplitude as the perturbation parameter. The thinning and subsequent breakup of the liquid sheet was associated to the generation of dilatational mode as the first harmonic, which gets superimposed over the fundamental sinuous mode. The dilatational mode thus contributes the intensification of wave motion and breakup of liquid sheets. The thinning has also been considered in the nonlinear evolution of a liquid sheet by Tharakan and Ramamurthi.<sup>5</sup>

The recent work of Bremond *et al.*<sup>6</sup> showed that as the liquid travels through the undulating pattern, it experiences

centrifugal accelerations in the frame of reference of the liquid sheet, perpendicular to the sheet. These accelerations, due to the difference in the propagation velocities of surface waves and the liquid, triggered a secondary instability and amplified the wave growth. The mechanism was called as “wavy corridor.” Although the work does not explicitly mention about the dilatational mode, the implication of the wavy corridor can be interpreted as switch in the mode from sinuous to dilatational due to the centrifugal acceleration. There could be a substantial improvement in atomization if the growth of the dilatational wave mode could be incorporated through a suitable mechanism of velocity gradient in the liquid sheet.

The acceleration normal to the direction of travel of the liquid sheet in the frame of reference of the sheet could also be achieved by suitably manipulating the initial velocity profile in the sheet. The present effort addresses the possibilities of obtaining the dilatational mode by means of inducing specific velocity profiles in the liquid sheet. The dilatational mode can come from different magnitudes of convective acceleration normal to the direction of propagation of the sheet in the frame of reference of the liquid.

Considering the liquid sheet to be thin, the usual assumption in literature has been to assume a constant axial velocity across its thickness, except Ibrahim<sup>7,8</sup> who studied the effect of parabolic and linear velocity profiles on the instability of liquid sheets. The velocity profiles chosen for their study reduced the growth of the sinuous and dilatational modes of the oscillations. The decrease in the relative velocity between the liquid and gas media at the interface was reported as the reason for the reduction in the instability. However, investigations of Wakimoto and Azuma<sup>9</sup> showed that the disturbance due to an inflectional velocity profile inside the radially expanding liquid sheet, reported as internal instability, led to the formation of disturbance wave on the surface. The instability of a liquid sheet is investigated

<sup>a)</sup>Author to whom correspondence should be addressed. Electronic mail: krmurthi@iitm.ac.in.

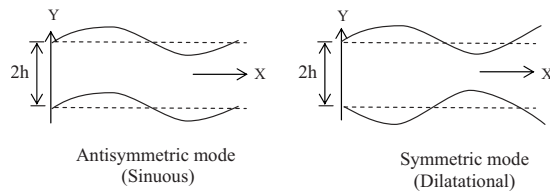


FIG. 1. Sinuous and dilatational disturbances.

for different axial velocity profiles and the possibility of inherent instability in the liquid sheet in the absence of the destabilizing aerodynamic forces is discussed.

## II. LINEAR STABILITY ANALYSIS CONSIDERING DIFFERENT VELOCITY PROFILES

### A. Model and velocity profiles

Consider an inviscid liquid sheet of thickness  $2h$  in a quiescent inviscid gas medium, as shown in Fig. 2. The liquid sheet is assumed to have an initial axial velocity profile  $U(y)$ . The velocity is very much smaller compared to the velocity of sound and thus both the liquid and gas phases are assumed to be incompressible. The amplitude  $\eta$  of the developing sinuous and dilatational wave modes is also taken to be much smaller than the thickness of the sheet.

The growth of the small perturbation  $\eta$  for different axial velocity profiles in the sheet is considered. The analysis follows the well established methodology of temporal stability analysis of Squire.<sup>1</sup> The dispersion relations which show the propagation of different wavelengths at different speeds are obtained for different velocity profiles. The velocity profiles shown in Fig. 3 are considered for the study, which are represented by the following equations in dimensionless form.

- (i) Linear profile A: an increase in velocity from the interface to the center line of the sheet, represented by

$$U = \alpha(1 \mp \beta y) \quad ('- ' \text{ for } y > 0 \text{ and } '+ ' \text{ for } y < 0)$$

$$\text{and } \alpha = \frac{U_{\max}}{U_{\text{av}}} = \frac{2}{2 - \beta}. \tag{1}$$

- (ii) Parabolic profile B: an increase in velocity from the interface to the center line of the sheet, represented by

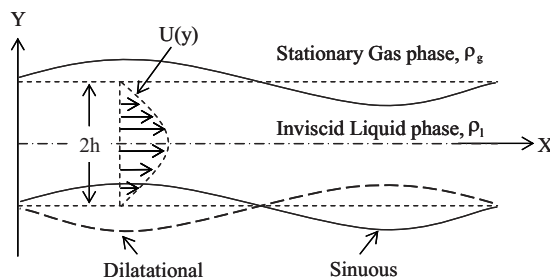


FIG. 2. Physical model.

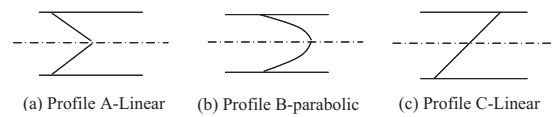


FIG. 3. Velocity profiles considered for the study.

$$U = \alpha(1 - \beta y^2), \quad \text{where } \alpha = \frac{U_{\max}}{U_{\text{av}}} = \frac{3}{3 - \beta}, \tag{2}$$

where  $U_{\max}$  and  $U_{\text{av}}$  are the maximum velocity and the average velocity of the velocity profile, respectively. It must be noted that as  $\beta$  goes from 1 to 0, flatter profiles are generated.

- (iii) Profile C: a linear increase in velocity from the lower interface to the upper interface, represented by

$$U = 1 + \beta y, \tag{3}$$

where  $\beta \leq 1$  for velocity to be always positive.

### B. Governing equations

The governing equations and boundary conditions are identical to those derived by Ibrahim<sup>7</sup> and Wakimoto and Azuma.<sup>9</sup> The equations are linearized and the procedure of linear stability analysis is followed. The axial velocity profiles within the liquid sheet are incorporated. Consider  $u'_i$  and  $v'_i$  to be the velocity components of the disturbances in the  $x$  and  $y$  directions, respectively, and  $p'_i$  be the pressure resulting from the disturbance. Here  $i=1$  and  $2$  represent the liquid and gas quantities, respectively. The equations of mass and momentum conservation that govern the liquid and gas medium are linearized to give

$$\frac{\partial u'_i}{\partial x} + \frac{\partial v'_i}{\partial y} = 0, \tag{4}$$

$$\frac{\partial u'_i}{\partial t} + \delta_{i1} \left( U \frac{\partial u'_i}{\partial x} + v'_i \frac{\partial U}{\partial y} \right) = - \frac{\rho_i}{\rho_l} \frac{\partial p'_i}{\partial x}, \tag{5}$$

$$\frac{\partial v'_i}{\partial t} + \delta_{i1} \left( U \frac{\partial v'_i}{\partial x} \right) = - \frac{\rho_i}{\rho_l} \frac{\partial p'_i}{\partial y}, \tag{6}$$

where  $\delta_{i1}$  is 1 or 0 depending on whether  $i=1$  or  $2$ .

Taking the partial derivative of Eq. (5) with respect to  $y$  and that of Eq. (6) with respect to  $x$ , subtracting the two resulting equations and using Eq. (4) gives

$$\left( \frac{\partial}{\partial t} + \delta_{i1} U \frac{\partial}{\partial x} \right) \left( \frac{\partial u'_i}{\partial y} - \frac{\partial v'_i}{\partial x} \right) + \delta_{i1} v'_i \frac{\partial^2 U}{\partial y^2} = 0. \tag{7}$$

The disturbance stream function is related to the disturbance velocity components following Ibrahim,<sup>7</sup>

$$u'_i = \frac{\partial \psi'_i}{\partial y}, \quad v'_i = - \frac{\partial \psi'_i}{\partial x}, \tag{8}$$

which satisfies Eq. (4). The disturbance stream function is represented in the form

$$\psi_i = \psi_i(y) \exp(iKx + \omega t), \quad (9)$$

where  $\psi_i(y)$  is a function of  $y$  only,  $K$  is the dimensionless wave number,  $t$  is dimensionless time, and  $\omega$  is the dimensionless complex frequency given by  $\omega = \omega_r + i\omega_i$ , where  $\omega_r$  is the dimensionless growth rate and  $\omega_i$  is  $2\pi$  times the dimensionless disturbance frequency. The average velocity across the sheet  $U_{av}$  and the sheet thickness  $h$  are used to make the different variables dimensionless. The stream function, wave number, and time (and complex frequency) are made dimensionless using  $hU_{av}$ ,  $h$ , and  $h/U_{av}$ , respectively. The resulting Rayleigh equation obtained by substituting Eqs. (8) and (9) into Eq. (7) is

$$(\omega + \delta_{ii}KU) \left( \frac{d^2 \psi_i}{dy^2} - K^2 \psi_i \right) - \delta_{ii}iK \frac{\partial^2 U}{\partial y^2} \psi_i = 0. \quad (10)$$

### C. Boundary conditions

The boundary conditions for Eq. (10) depend on whether the sheet disturbance is sinuous or dilatational. The amplitude of the disturbance at the two interfaces in dimensionless form, for sinuous and dilatational modes in order, is given by

$$y_+ = 1 + \eta, \quad y_- = -1 + \eta, \quad (11)$$

and

$$y_+ = 1 + \eta, \quad y_- = -1 - \eta. \quad (12)$$

Here, the subscripts  $+$  and  $-$  represent the conditions for upper and lower interfaces, respectively, and  $\eta$  is the amplitude of disturbance at the interface. For sinuous disturbances, the linearized boundary conditions showing the pressure balance and the kinematic condition at the two interfaces  $y = \pm 1$  are respectively given by

$$-p'_l = -p'_g + p'_\sigma, \quad (13)$$

$$v'_i = \frac{\partial \eta}{\partial t} + \delta_{ii}U \frac{\partial \eta}{\partial x}. \quad (14)$$

The effects of the disturbance in the gas will vanish far away from the liquid sheet and thus

$$v'_2 = 0 \quad \text{as } y \rightarrow \pm \infty. \quad (15)$$

For dilatational disturbances, the only boundary condition that changes form is the liquid kinematic boundary condition at  $y = -1$  which becomes

$$v'_1 = - \left( \frac{\partial \eta}{\partial t} + U \frac{\partial \eta}{\partial x} \right) \quad \text{at } y = -1. \quad (16)$$

Here,  $\eta$  is the interface displacement given by  $\eta = \eta_0 \exp(iKx + \omega t)$ , where  $\eta_0$  is the amplitude of the initial interface displacement.  $p'$  is the pressure due to the disturbance and is made dimensionless by  $\rho_l U_{av}^2$ , where  $\rho_l$  is the liquid density. The dimensionless surface tension pressure  $p'_\sigma$  is obtained as  $p'_\sigma = 1/We$ , with  $We$  being the Weber number of curvature of the liquid-gas interface given by  $We = (\partial^2 \eta / \partial x^2)^{-1}$  and  $We$  being the Weber number of liquid defined based on the average velocity of the velocity profile as  $We = \rho_l U_{av}^2 h / \sigma$ , where  $\sigma$  is surface tension.

### D. Method of solution

The disturbance stream function for the gas medium remains unaltered for all velocity profiles mentioned in Fig. 3 and is seen from Eq. (10) to give the following closed form solution:

$$\psi_2 = {}^2C_0 e^{Ky} + {}^2C_1 e^{-Ky}. \quad (17)$$

The pressure distribution in the liquid for linear profiles  $A$  and  $C$  give a closed form solution for disturbance stream function in the form

$$\psi_1 = {}^{1,A,C}C_0 e^{Ky} + {}^{1,A,C}C_1 e^{-Ky}. \quad (18)$$

However, for profile  $B$ , a closed form solution is not possible and a power series solution of the form  $\psi = \sum_{n=0}^{\infty} A_n y^n$  (used by Ibrahim<sup>7</sup>) is assumed. Substituting this series solution into Eq. (10) and equating the distinct powers of  $y$  to zero, we obtain

$$A_2 = \frac{(K^2 \varepsilon - 2\beta)A_0}{2\varepsilon}, \quad A_3 = \frac{(K^2 \varepsilon - 2\beta)A_1}{6\varepsilon}, \quad \text{and}$$

$$A_{n+2} = \frac{\{[n(n-1)\beta + K^2 \varepsilon - 2\beta]A_n - K^2 \beta A_{n-2}\}}{\varepsilon(n+2)(n+1)}$$

for  $n \geq 2$ ,

where  $\varepsilon = \omega / iK\alpha + 1$ .

Thus, the stream function for profile  $B$  takes the form

$$\psi = {}^{1,B}C_0 \left[ A_0 \left( 1 + \frac{(K^2 \varepsilon - 2\beta)}{2\varepsilon} y^2 + \sum_{n=2}^{\infty} \frac{A_{n+2}}{A_0} y^{n+2} \right)_{n=\text{even}} \right] + {}^{1,B}C_1 \left[ A_1 \left( y + \frac{(K^2 \varepsilon - 2\beta)A_1}{6\varepsilon} y^3 + \sum_{n=3}^{\infty} \frac{A_{n+2}}{A_1} y^{n+2} \right)_{n=\text{odd}} \right]. \quad (19)$$

The boundary conditions (14) and (15) are used to evaluate the constants of integration  ${}^2C_0$ ,  ${}^2C_1$ ,  ${}^{1,A}C_0$ ,  ${}^{1,A}C_1$ ,  ${}^{1,B}C_0$ ,  ${}^{1,B}C_1$ ,  ${}^{1,C}C_0$ , and  ${}^{1,C}C_1$ , in Eqs. (17)–(19). Here, the superscripts  $A$ ,  $B$ , and  $C$  correspond to profiles  $A$ ,  $B$ , and  $C$ , and 1 and 2 correspond to liquid and gas phases, respectively.

It must be noted that profile  $C$  is subjected to different conditions of velocity on both the interfaces. This manifests by a phase difference  $\theta$  between the two surface waves at the gas-liquid interfaces giving rise to parasymmetric and parantisymmetric wave modes. The boundary conditions mentioned in Eqs. (13)–(16) remain the same, except that the disturbance amplitudes on both the interfaces are different, thus giving rise to an additional parameter called displacement ratio.

Using linearized  $x$ -momentum equation relating stream function and pressure,  $\partial u'_i / \partial t + \delta_{ii}(U \partial u'_i / \partial x + v'_i \partial U / \partial y) = -(\rho_l / \rho_g)(\partial p'_i / \partial x)$ , where  $u'_i = \partial \psi_i / \partial y$ , the liquid and gas pressures are evaluated. These expressions for pressure,

when substituted into Eq. (13), yield the dispersion relations which relate the wave number and growth rate for the different velocity profiles.

**E. Dispersion relations for the different velocity profiles**

**1. Linear profile A**

The dispersion relation for sinuous mode is determined as

$$(\Omega + iK\gamma\sqrt{We})^2 \tanh K + \frac{2i\beta\sqrt{We}}{(2-\beta)}(\Omega + iK\gamma\sqrt{We}) + \rho\Omega^2 + K^3 = 0. \tag{20a}$$

By separating real and imaginary parts of Eq. (20a) we get

$$\Omega_i = - \frac{\sqrt{We}[\beta + 2(1-\beta)K \tanh K]}{(\tanh K + \rho)(2-\beta)} \tag{20b}$$

and

$$\Omega_r = \sqrt{\Omega_i^2 + \frac{\gamma K \sqrt{We} \tanh K (2\Omega_i + \gamma K \sqrt{We}) + \frac{2\beta\sqrt{We}}{(2-\beta)}(\Omega_i + \gamma K \sqrt{We}) - K^3}{(\tanh K + \rho)}}. \tag{20c}$$

The above equation is different from that obtained by Ibrahim<sup>8</sup> as the term  $(\Omega_i - \gamma K \sqrt{We})$  is used instead of  $(\Omega_i + \gamma K \sqrt{We})$ .

In the case of the dilatational mode, we get

$$(\Omega + iK\gamma\sqrt{We})^2 \coth K + \frac{2i\beta\sqrt{We}}{(2-\beta)}(\Omega + iK\gamma\sqrt{We}) + \rho\Omega^2 + K^3 = 0, \tag{21}$$

where  $\Omega = \omega\sqrt{We}$ ,  $We = \rho_l U_{av}^2 h / \sigma$  is the Weber number of the liquid defined based on the average velocity,  $\rho = \rho_g / \rho_l$  is the gas to liquid density ratio, and  $\gamma = 2(1-\beta)/(2-\beta)$ .

**2. Parabolic profile B**

The dispersion relation for sinuous mode for the parabolic profile is determined as

$$\left(\frac{C_2}{kC_0}\right)[\Omega + iK\alpha(1-\beta)\sqrt{We}]^2 + 2i\alpha\beta\sqrt{We}[\Omega + iK\alpha(1-\beta)\sqrt{We}] + \rho\Omega^2 + K^3 = 0. \tag{22}$$

For the dilatational mode the dispersion relation becomes

$$\left(\frac{C_3}{kC_1}\right)[\Omega + iK\alpha(1-\beta)\sqrt{We}]^2 + 2i\alpha\beta\sqrt{We}[\Omega + iK\alpha(1-\beta)\sqrt{We}] + \rho\Omega^2 + K^3 = 0, \tag{23}$$

where

$$C_1 = \left(1 + \frac{(K^2\varepsilon - 2\beta)}{6\varepsilon} + \sum_{n=3}^{\infty} A_{n+2}\right)_{n=odd},$$

$$C_3 = \left(1 + \frac{(K^2\varepsilon - 2\beta)}{2\varepsilon} + \sum_{n=3}^{\infty} (n+2)A_{n+2}\right)_{n=odd},$$

$$C_0 = \left(1 + \frac{(K^2\varepsilon - 2\beta)}{2\varepsilon} + \sum_{n=2}^{\infty} A_{n+2}\right)_{n=even},$$

and

$$C_2 = \left(\frac{(K^2\varepsilon - 2\beta)}{\varepsilon} + \sum_{n=2}^{\infty} (n+2)A_{n+2}\right)_{n=even},$$

and

$$\Omega = \omega\sqrt{We}, \quad \rho = \rho_g / \rho_l, \quad \varepsilon = \omega / iK\alpha + 1.$$

**3. Linear profile C with monotonic increase in velocity from lower to upper interface**

Since the two gas-liquid interfaces are subjected to different velocities, they have a different dispersion relation containing an additional parameter, viz., a displacement ratio  $\chi$  following Lin.<sup>10</sup> The dispersion relation governing the upper interface is given by

$$-[P - \chi Q] = \left(\rho\omega^2 + \frac{K^3}{We}\right) \sinh(2K), \tag{24}$$

while the dispersion relation governing the lower interface is given by

$$\left[\frac{Q}{\chi} - R\right] = \left(\rho\omega^2 + \frac{K^3}{We}\right) \sinh(2K), \tag{25}$$

where

$$P = (\omega + iKU_a)\{(\omega + iKU_a)\cosh(2K) - i\beta \sinh(2K)\},$$

$$Q = (\omega + iKU_a)(\omega + iKU_b),$$

$$R = (\omega + iKU_b)\{(\omega + iKU_b)\cosh(2K) + i\beta \sinh(2K)\},$$

$\chi = \eta_{02} / \eta_{01}$  is the amplitude ratio, and  $U_a$  and  $U_b$  are the dimensionless velocities at upper and lower interfaces given by  $(1+\beta)$  and  $(1-\beta)$ , respectively.

Eliminating  $\chi$  from Eqs. (24) and (25), we get a fourth degree polynomial in  $\omega$ ,

$$\frac{\left(\rho\omega^2 + \frac{K^3}{We}\right)\sinh(2K) + P}{Q} = \frac{Q}{\left(\rho\omega^2 + \frac{K^3}{We}\right)\sinh(2K) + R}. \quad (26)$$

Choosing  $a = \omega + iK$ ,  $b = iK\beta$ , we obtain a fourth degree polynomial in  $a$  as

$$C_0a^4 + C_1a^3 + C_2a^2 + C_3a + C_4 = 0, \quad (27)$$

where

$$C_0 = u^2 - 1,$$

$$C_1 = -2uw,$$

$$C_2 = 2ux - v^2 + w^2 + 2b^2,$$

$$C_3 = -2wx,$$

$$C_4 = x^2 - b^4,$$

where

$$u = \cosh(2K) + \rho \sinh(2K),$$

$$v = 2b \cosh(2K) - i\beta \sinh(2K),$$

$$w = 2iK\rho \sinh(2K),$$

$$x = b^2 \cosh(2K) + (K^3/We - \rho K^2)\sinh(2K) - i\beta b \sinh(2K).$$

It was observed that the dispersion relation remains the same for dilatational mode. Of the four possible roots, two pertain to sinuous mode and the other two roots correspond to dilatational mode.

These dispersion relations (20) and (21) for the linear velocity profile A, Eqs. (22) and (23) for the parabolic velocity profile B, and Eq. (27) for the linearly varying velocity from the lower to upper interface were solved for the complex frequency in MATLAB for varying values of wave number. Different dispersion plots were obtained and are discussed subsequently.

## F. Limiting solutions

Upon substitution of  $\beta=0$  in Eqs. (20a)–(20c) and (21)–(23) the following classic results of Squire<sup>1</sup> and Hagerty and Shea<sup>2</sup> for linear stability of a liquid sheet of uniform profile are recovered:  $(\Omega + iK\sqrt{We})^2 \tanh K + \rho\Omega^2 + K^3 = 0$  for sinuous mode and  $(\Omega + iK\sqrt{We})^2 \coth K + \rho\Omega^2 + K^3 = 0$  for dilatational mode.

Substituting  $\beta=0$  in Eq. (27) yields  $b=0$  and  $P=R$ , thus transforming Eq. (26) as

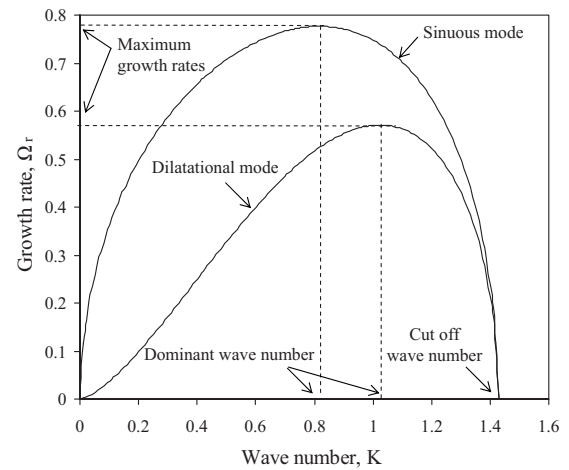


FIG. 4. Variation of nondimensional growth rate with nondimensional wave number for sinuous and dilatational modes at  $We=1400$  and  $\rho=0.001$ .

$$\left(\rho\omega^2 + \frac{K^3}{We}\right)\sinh(2K) + P = \pm Q, \quad (28)$$

where  $P = (\omega + iK)^2 \cosh(2K)$  and  $Q = (\omega + iK)^2$ .

Substituting  $P$  and  $Q$  into Eq. (28), we get

$$\begin{aligned} \left(\rho\omega^2 + \frac{K^3}{We}\right)\sinh(2K) + (\omega + iK)^2 \cosh(2K) \\ = \pm (\omega + iK)^2. \end{aligned} \quad (29)$$

Considering positive root in Eq. (29) yields

$$(\omega + iK)^2 [\cosh(2K) - 1] + \left(\rho\omega^2 + \frac{K^3}{We}\right)\sinh(2K) = 0, \quad (30)$$

which gives

$$\begin{aligned} (\omega + iK)^2 (2 \sinh^2 K) + \left(\rho\omega^2 + \frac{K^3}{We}\right) (2 \sinh K \cosh K) \\ = 0. \end{aligned} \quad (31)$$

On simplification we get  $(\omega + iK)^2 \tanh K + [\rho\omega^2 + (K^3/We)] = 0$ .

Substituting  $\Omega = \omega\sqrt{We}$  in the above expression, we obtain the following dispersion relation:

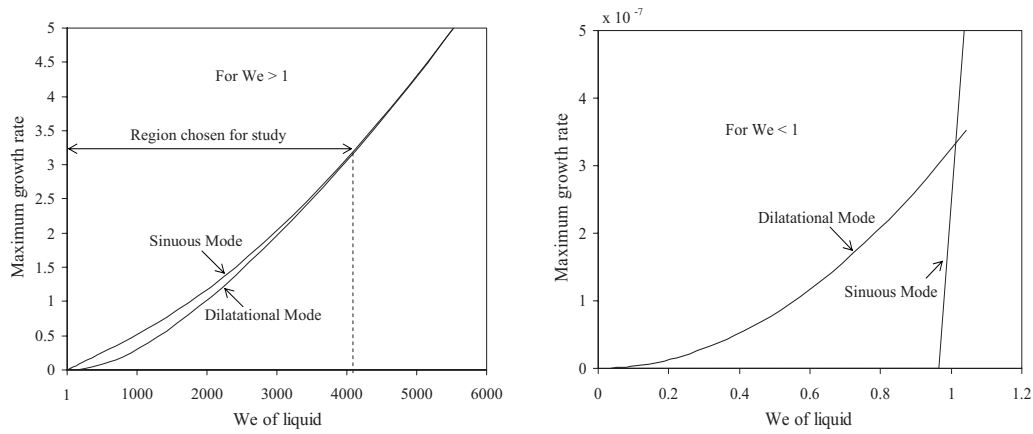
$$(\Omega + iK\sqrt{We})^2 \tanh K + (\rho\Omega^2 + K^3) = 0, \quad (32)$$

which is identical to the dispersion equation given by Squire.

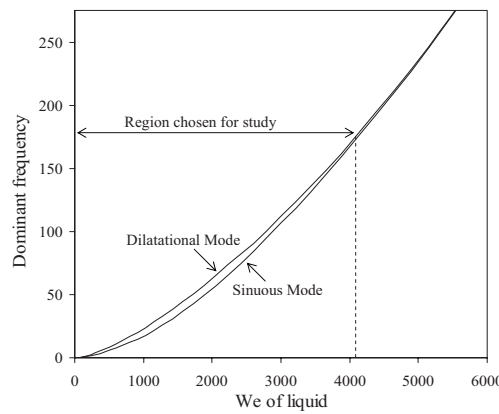
Similarly if negative root in Eq. (29) is considered,

$$\begin{aligned} (\omega + iK)^2 [\cosh(2K) + 1] + \left(\rho\omega^2 + \frac{K^3}{We}\right)\sinh(2K) = 0, \\ \end{aligned} \quad (33)$$

which gives



(a) Maximum non dimensional growth rate



(b) Dominant non dimensional frequency

FIG. 5. Effect of the Weber number growth rate and dominant frequency of sinuous and dilatational modes.

$$(\omega + iK)^2(2 \cosh^2 K) + \left( \rho\omega^2 + \frac{K^3}{We} \right)(2 \cosh K \sinh K) = 0. \tag{34}$$

On simplification, the following dispersion relation for dilatational waveform is obtained:

$$(\Omega + iK\sqrt{We})^2 \coth K + (\rho\Omega^2 + K^3) = 0. \tag{35}$$

Equation (32) for the positive root and Eq. (35) for the negative root are identical to dispersion relations given by Squire<sup>1</sup> for sinuous and dilatational modes, respectively. Weber number and gas to liquid density ratio influence the stability.

### III. RESULTS AND DISCUSSION

We study the dispersion relations given by Eqs. (20a)–(20c) and (21)–(23) and the asymptotic behavior of the dispersion relation given in Eq. (27) for different values of  $\beta$  for a range of wavelengths. The results with  $\beta=0$  are first carried out which enable us to identify and classify the eigenvalues of the system, and gain an insight into the physical nature of the instability.

#### A. Uniform velocity profile ( $\beta=0$ )

Figure 4 shows the dispersion plot for sinuous and dilatational modes at  $We=1400$  and  $\rho=0.001$ . It is seen that the growth rate of sinuous mode is considerably higher compared to that of dilatational mode. Beyond a cutoff wave number, growth is not observed due to the stabilizing effect of surface tension. The waves below the cutoff wave number are unstable due to aerodynamic forces. The maximum growth rate for the dilatational mode is obtained at higher dimensionless wave numbers than for the sinuous mode. This gives the dominant frequency of the dilatational modes to be higher than for the sinuous mode. The dominant frequency is defined as the frequency which provides the maximum possible growth rate.

The maximum growth rates and the dominant frequencies of sinuous and dilatational modes for  $\rho=0.001$  are plotted in Figs. 5(a) and 5(b), respectively. Over a range of Weber numbers up to about 4000, the maximum growth rate of sinuous mode is larger than dilatational mode and the dominant frequency of dilatational mode is greater than sinuous mode.

A special mention to  $We < 1$  is essential at this stage. It is observed that for  $We < 1$ , maximum growth rate of dilata-

tional mode is larger while the sinuous modes do not grow. The spatial-temporal analysis of Lin,<sup>11</sup> however, shows that the sinuous mode is absolutely unstable for  $We < 1$ . The analysis considers perturbations to grow both in space and time, thus allowing the wave number  $K$  to be complex and reveals a new zone of instability, known as “absolute instability.” This instability is observed only for  $We < 1$  during which the disturbances tend to propagate in both upstream and downstream directions, as the inertia is not sufficiently large to carry down all the unstable disturbances. A pure temporal analysis cannot explore this region and gives the impression that the growth of sinuous mode is absent. This was also addressed for liquid jets by Dumouchel.<sup>12</sup>

For  $We \gg 1$ , the perturbations propagate only in the downstream direction and the instability is known as “convective instability.” Weber numbers greater than 1.0 are considered in the present analysis for which the temporal analysis would therefore be adequate.

The maximum growth rate of both the modes is seen from Figs. 5(a) and 5(b) to be about the same when  $We > 4000$ . At higher Weber numbers, the wavelengths of the dominant waves are very small compared to the thickness of the sheet. Thus, it would be expected that only a thin region around each interface will be affected by surface disturbances. This allows the two surfaces to become independent of each other, and both of them have a similar growth rate. The region of interest would therefore be up to about  $We < 4000$  and this is the region chosen for analysis.

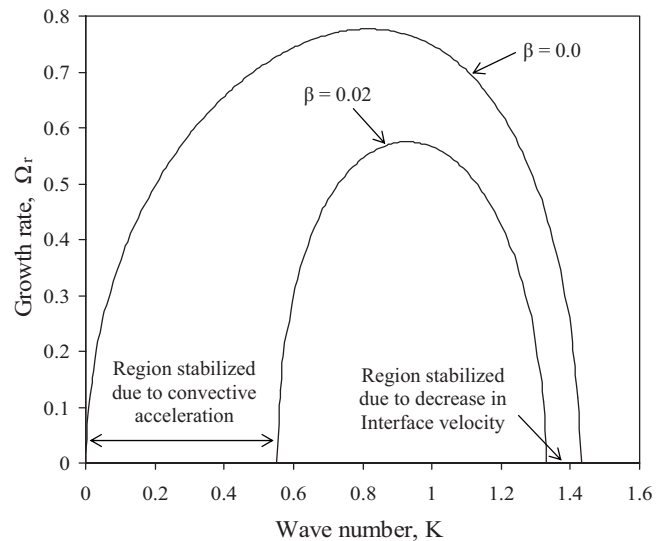
### B. Profile A: Linear with varying values of $\beta$

Figure 6 shows the effect of profile A on the maximum growth rate of liquid sheet, for  $We=1400$ ,  $\rho=0.001$ , and  $\beta=0.02$ . Compared to a uniform velocity profile, there is a decrease in maximum growth rate of sinuous and dilatational modes, as shown in Figs. 6(a) and 6(b), respectively. The range of wavelengths within which waves grow was also found to decrease. Interestingly, the longer waves were also found to stabilize, thus imposing a lower limit on the wave number beyond which waves can grow.

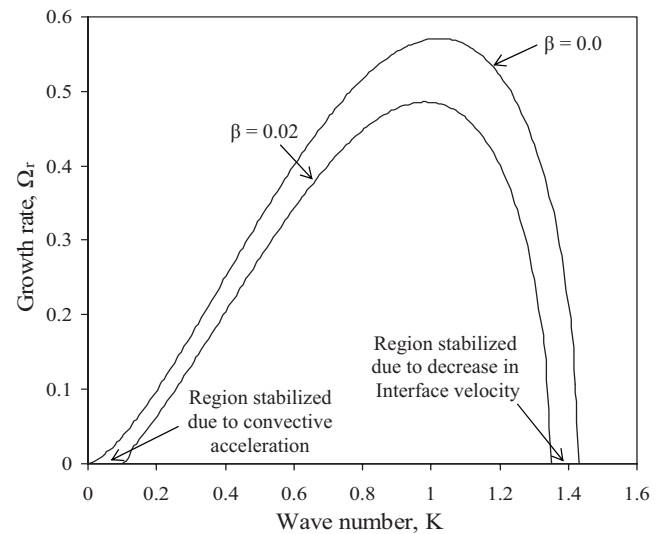
The physical reason can be explained by examining the following expression obtained for liquid pressure:

$$p'_l = \frac{-\eta_0(\omega + iK\gamma)}{K \cosh(K)} \times \left[ (\omega + iKU) \sinh(Ky) \pm \frac{2i\beta}{(2-\beta)} \cosh(Ky) \right]. \quad (36)$$

Of the two terms in the parenthesis, the first term is an exclusive function of gas-liquid interface velocity while the second term is the convective acceleration due to gradient of velocity profile in the frame of reference of the liquid sheet. The second term is the outcome of  $v'_1 \partial U / \partial y$  in Eq. (5) pertaining to  $x$ -momentum equation. The magnitude of this convective acceleration is a direct function of the gradient of velocity profile and decreases from the center line of the sheet to a minimum at the interfaces. This acceleration, which opposes the liquid pressure, is found to dominate at low wave numbers, thus stabilizing the long waves. How-



(a) Non dimensional growth rate in Sinuous mode



(b) Non dimensional growth rate in Dilatational mode

FIG. 6. Effect of profile A for  $We=1400$ ,  $\rho=0.001$ , and  $\beta=0.02$  on sinuous and dilatational modes.

ever, the smaller waves are affected by a decrease in the interface velocity, apart from the stabilizing effect of surface tension. Hence, the minimum wave number is decided by the convective acceleration due to velocity gradient, while the maximum wave number is decided by the combined effect of a decrease in interface velocity and surface tension. Note that the additional force due to convective acceleration can be either stabilizing or destabilizing based on the type of velocity profile incorporated within the liquid sheet.

The dispersion plots obtained by present analysis are compared to that of Ibrahim,<sup>8</sup> shown dotted, for  $We=10\,000$  and  $\rho=0.01$  in Fig. 7. For both  $\beta=0.04$  and  $\beta=0.08$ , the sheet is found to be stabilized over a smaller range of wave numbers as compared to the predictions of Ibrahim.<sup>8</sup> The present analysis shows that at higher density ratios and larger Weber numbers, the stable region until the lower limiting wave number remains invariant. This conclusion could have been obtained in Ibrahim's<sup>8</sup> work but for the

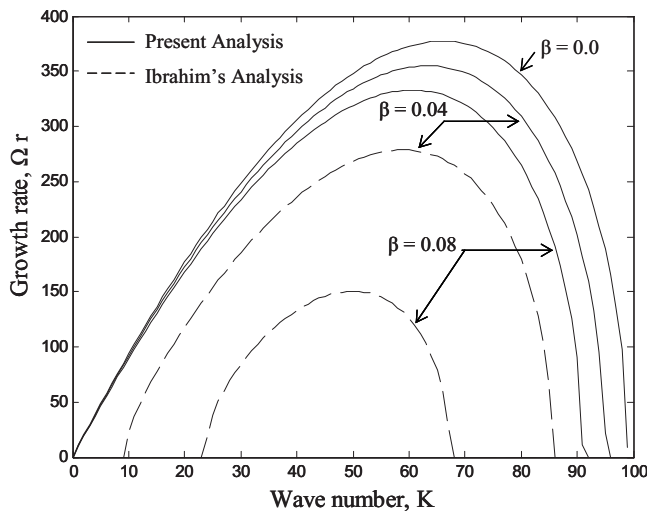


FIG. 7. Comparison of dispersion plots obtained by present analysis with that of Ibrahim for  $We=10\,000$  and  $\rho=0.01$ .

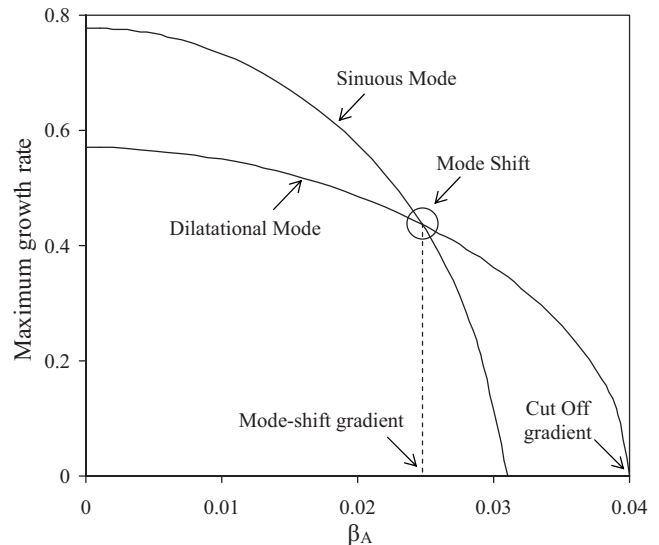
oversight in using the expression  $(\Omega_i - \gamma K \sqrt{We})$  instead of  $(\Omega_i + \gamma K \sqrt{We})$ , dealt with earlier. The initial stable region was seen in their analysis to be valid at larger wave numbers and predicted the sheet to be completely stable at low value of  $\beta=0.1$ .

Figure 8 gives the variation of the maximum growth rate and dominant frequency as the gradient of the velocity profile  $A$  is changed from 0 to 0.04, for  $We=1400$  and  $\rho=0.001$ . The maximum growth rate for the sinuous mode decreased rapidly compared to dilatational mode. This resulted in a mode shift from sinuous to dilatational mode beyond a mode-shift gradient. A cutoff gradient beyond which growth is not noticed is also seen to exist. While the dominant frequency of sinuous mode increased, the dominant frequency of dilatational mode decreased with the increase in the gradient  $\beta$ . Just beyond the mode-shift gradient, dilatational mode is achieved at a higher value of dominant frequency.

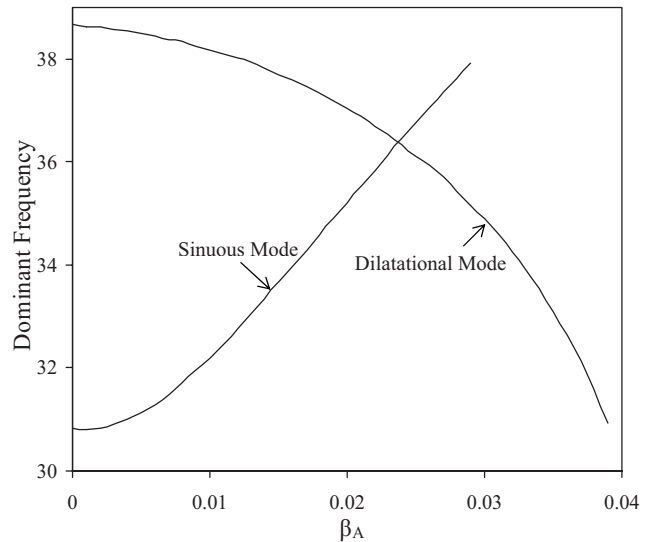
**C. Profile B: Parabolic**

The variation of growth rate and frequencies of parabolic profile were similar to those of profile  $A$ , dealt in Sec. III B. The ratio of maximum growth rate of linear and parabolic profiles with density ratio is plotted in Fig. 9 for varying gradient of the profiles. Both the mean and interface velocities are kept constant for comparison. This is ensured by appropriately choosing the gradient of both profiles  $\beta_B = 3\beta_A / (4 - \beta_A)$ , where  $\beta_A$  and  $\beta_B$  are the gradients of the linear velocity profile  $A$  and parabolic profile  $B$  at the interface.

Irrespective of the gradient of the velocity profiles, the ratio approaches 1.0 with increasing density ratio thus showing that velocity distribution has a profound effect only at lower density ratios, which gives lower dominant wave numbers. The ratio approaches 1.0 at higher density ratios since the relative interface velocity, which influences higher wave numbers, is kept constant for comparison. The stabilization



(a) Maximum non dimensional growth rate



(b) Dominant non dimensional frequency

FIG. 8. Influence of gradient of profile  $A$  for  $We=1400$  and  $\rho=0.001$  on maximum growth rate and dominant frequency of sinuous and dilatational modes.

due to convective acceleration is greater in the case of profile  $B$  due to larger gradient at the interface, compared to profile  $A$ .

It is of interest to determine the effect of decreasing the gas density to very low values such that the aerodynamic shear is absent. Substituting  $\rho=0$  in the dispersion relations given in Eqs. (20a)–(20c) and (21)–(23) shows that the liquid sheets with linear profile  $A$  or parabolic profile  $B$  within its thickness can never grow in the absence of gas medium. The stability results in view of the convective acceleration acting on the sheet going to zero. Even if the gradient of velocity profile is reversed to give maximum velocities at the interface and minimum at the center line, as illustrated in Fig. 10, the growth does not take place. Any velocity profile symmetric at the center line of the sheet is therefore stable in the absence of gas medium. However, compared to flat profile, an increase in growth rate is observed for this reversed ve-

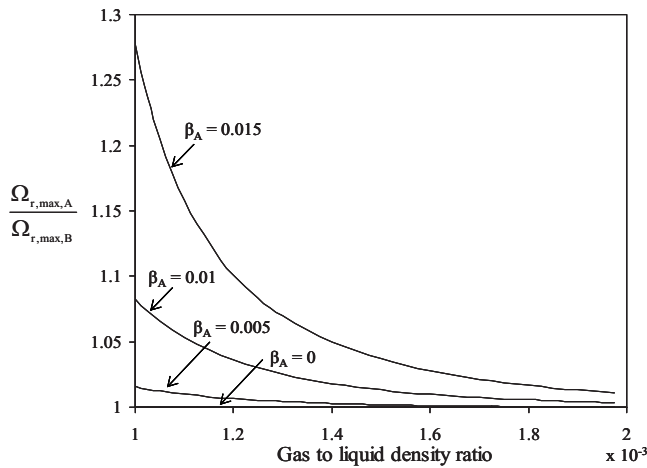


FIG. 9. Effect of density ratio on the ratio of maximum growth rate of profiles A and B for  $We=1400$ .

locity profile (when the gradient is negative) at larger Weber numbers and density ratios. This increase is shown in Fig. 11 and is due to the increase in the interface velocity. The influence of interface velocity becomes more conspicuous at higher wave numbers.

**D. Profile C-linear: Internal instability**

The limiting solution of dispersion relation of profile C given in Eq. (26), under the negligible effect of aerodynamic and surface tension effects gives  $PR=Q^2$ . Solving this equation for complex frequency gives the following roots:

$$\omega_1^\pm = -iK \pm iK\beta \quad \text{and}$$

$$\omega_2^\pm = -iK \pm \beta \sqrt{\frac{2K}{\tanh(2K)} - (K^2 + 1)}.$$

The first set of roots representing dilatational mode is stable but the positive root in the second set can grow depending on the sign of the term under the square root. Wave numbers satisfying the condition  $2K/\tanh(2K) > (K^2 + 1)$  grow with time and the mode is essentially sinusoidal. Thus, profile C is unstable even in the absence of a gas medium. Since the velocity on both interfaces is different, the net convective acceleration in transverse direction due to velocity gradient is found responsible to destabilize the sheet.

As an example, the dispersion plots with varying gradients of linear velocity profile are shown in Fig. 12 for  $We=1400$ . The surface tension opposes the net convective acceleration on the sheet and thus a critical gradient of ve-

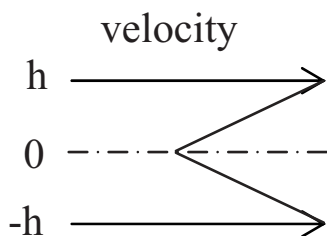


FIG. 10. Reversed velocity profile with maximum velocity at interface.

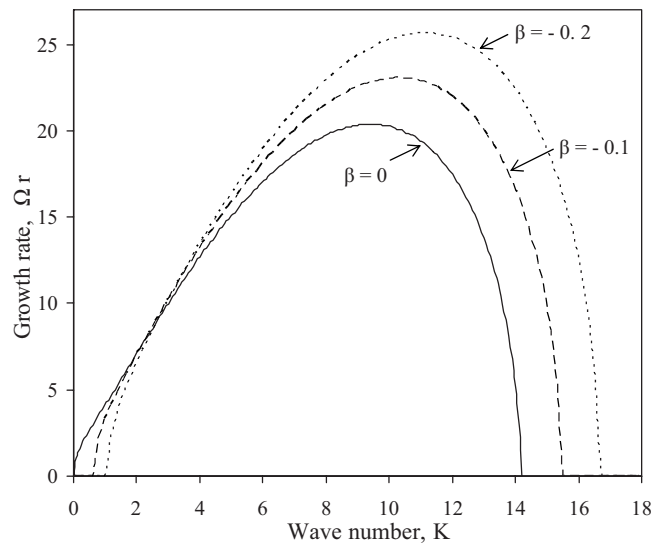


FIG. 11. Dispersion plot for velocity profile with negative gradient at  $We=1400$  and  $\rho=0.01$ .

locity profile ( $\beta=0.046$ ) is seen necessary for the sheet to destabilize (Fig. 12). The critical gradient is found to be independent of the average velocity of the liquid sheet.

This trend is similar to the internal instability reported by Wakimoto and Azuma<sup>9</sup> for the specific case of radially expanding liquid sheet. The inflectional profile in the expanding sheet was mentioned to be responsible for instability in the absence of aerodynamic effect, following the Orr-Sommerfeld criterion for boundary layer instability. The present study shows that an inflectional profile is not the necessary criterion to destabilize a sheet in the absence of gas medium. Any profile, which can give a differential convective acceleration on both interfaces, can destabilize the sheet at lower wave numbers. An inflection profile becomes a necessary criterion in the case of a bounded flow, with rigid or free boundaries, as was suggested by Rayleigh. Since the

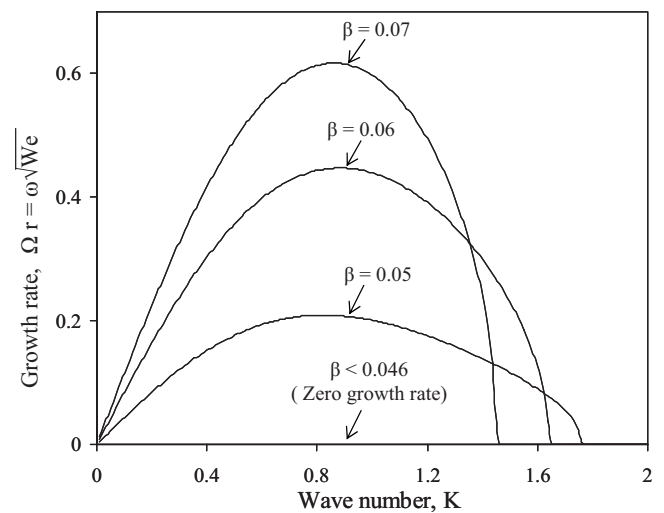


FIG. 12. Dispersion plot of linear velocity profile for increasing gradient for  $We=1400$ .

boundaries are subjected to kinematic boundary condition in the present work, any profile providing differential acceleration can cause the destabilization.

#### IV. CONCLUSIONS

Linear stability analysis of an inviscid liquid sheet having different velocity profiles across its thickness is reported. Liquid sheets for which the velocities change progressively between the two interfaces are demonstrated to be inherently unstable even in the absence of the destabilizing aerodynamic shear at the liquid-gas interfaces. The role of the convective acceleration in the frame of reference of liquid sheet is inferred to be an important parameter influencing the instability of the sheet.

For symmetric velocity profiles, the sheet is unstable only in the presence of the aerodynamic force at the interface. The waveforms are dominantly sinuous; however, with larger velocity gradients the dilatational modes are observed. The dilatational modes would strongly contribute to the atomization of the liquid sheets. The maximum growth rates and the range of wavelengths over which waves grow in the liquid sheet decrease as the gradient of symmetric velocity profiles increases. The convective acceleration from the velocity gradient is found to stabilize the longer waves while the growth of shorter waves is hampered by the combined effect of the surface tension and a decrease in the interface velocity between gas and liquid media.

Liquid sheets for which the velocities change progressively between the two interfaces are inherently unstable even in the absence of aerodynamic shear, such as when the liquid sheet is injected in vacuum. The instability arises from the differential convective acceleration at the two interfaces. The incorporation of such velocity profiles in liquid sheets could provide an effective means of atomization.

<sup>1</sup>H. B. Squire, "Investigation of the instability of a moving liquid film," *Br. J. Appl. Phys.* **4**, 167 (1953).

<sup>2</sup>W. W. Hagerty and J. F. Shea, "A study of the stability of plane fluid sheets," *ASME Trans. J. Appl. Mech.* **22**, 509 (1955).

<sup>3</sup>R. H. Rangel and W. A. Sirignano, "The linear and nonlinear shear instability of a fluid sheet," *Phys. Fluids A* **3**, 2392 (1991).

<sup>4</sup>S. A. Jazayeri and X. Li, "Nonlinear instability of plane liquid sheets," *J. Fluid Mech.* **406**, 281 (2000).

<sup>5</sup>T. J. Tharakan and K. Ramamurthi, "Nonlinear breakup of thin liquid sheets," *Acta Mech.* **156**, 29 (2002).

<sup>6</sup>N. Bremond, C. Clanet, and E. Villermaux, "Atomization of undulating liquid sheets," *J. Fluid Mech.* **585**, 421 (2007).

<sup>7</sup>E. A. Ibrahim, "Instability of a liquid sheet of parabolic velocity profile," *Phys. Fluids* **10**, 1034 (1998).

<sup>8</sup>E. A. Ibrahim, "Effect of velocity profile on liquid sheet instability," *Chem. Eng. Sci.* **52**, 4419 (1997).

<sup>9</sup>T. Wakimoto and T. Azuma, "Instability of radial liquid sheet flow," *JSME Int. J., Ser. B* **47**, 9 (2004).

<sup>10</sup>X. Li, "On the instability of plane liquid sheets in two gas streams of unequal velocities," *Acta Mech.* **106**, 137 (1994).

<sup>11</sup>S. P. Lin, *Breakup of Liquid Sheets and Jets* (Cambridge University Press, Cambridge, 2003), pp. 7–24.

<sup>12</sup>C. Dumouchel, "On the experimental investigation on primary atomization of liquid streams," *Exp. Fluids* **45**, 371 (2008).